J. Earth Syst. Sci. (2021)130 176
https://doi.org/10.1007/s12040-021-01696-x

Laboratory measurements of ultrasonic wave velocities of rock samples and their relation to log data: A case study from Mumbai offshore

Venkatesh Ambati, Shashank Sharma, M Nagendra Babu and Rajesh R Nair*

Petroleum Geomechanics Laboratory, Indian Institute of Technology Madras, Chennai, India.
**Corresponding author. e-mail: rajeshnair@iitm.ac.in*

MS received 18 April 2021; revised 22 June 2021; accepted 26 June 2021

The characterization of the reservoir rock's geomechanical properties is critical to address wellbore instabilities and subsidence-related issues. To address these issues, lab-derived dynamic and static elastic properties are essential to match the *in-situ* rock properties. In this study, as part of a new integrated workflow P-wave and S-wave velocities are congregated using ultrasonic transducers for the core plugs, which constitutes mainly carbonates, shales, and both. Mineral composition, shale anisotropy, seismic velocities, and cross plots are studied to understand shear wave splitting. During this study, as a part of 1D mechanical Earth models, rock elastic properties are calculated for 60 wells using petrophysical logs (gamma, density, acoustic and caliper). Also, triaxial loading tests are conducted on 14 specimens collected from the same wells, static Poisson's ratio and static Young's modulus are computed from the stress-strain curves. The major differences are observed between static and dynamic elastic properties calculated from well logs and lab tests. Cohesion and friction angle for rock samples are estimated from the triaxial tests under different confining pressures. The objective of this study is to compare the elastic properties derived from the ultrasonic method with well logs and fill the gaps in the 1D geomechanical model. The combined analysis of elastic properties from different methods provides exciting insights on wellbore stability in anisotropic rock.

Keywords. Rock properties; triaxial testing; ultrasonic measurements; mechanical Earth model; Mumbai offshore.

Nomenclature

PR_{dy}	Dynamic Poisson's ratio
E_{dyn}	Dynamic Young's modulus (GPa)
K	Bulk modulus (GPa)
G, μ	Shear modulus (GPa)
1D MEM	One-dimensional mechanical Earth model
V_p, υ_p	Compressional wave velocity (m/s)
V_s, υ_s	Shear wave velocity (m/s)
UVW	Ultrasonic wave velocity (m/s)
ISRM	International Society of Rock Mechanics
T_p	Travelling time (sec)
σ_1	Vertical load (psi)
σ_2, σ_3	Horizontal loads (psi)
kN	Kilo Newton
$\mathrm{C_o}$	Cohesion
μ_i	Coefficient of internal friction angle
ASTM	American Society for Testing and Materials
E_{sat}	Static Young's modulus

Published online: 25 August 2021

$UCS_{limestone}$	Unconfined compressive strength of limestone
UCS_{shale}	Unconfined compressive strength of shale
mD	Milli Darcy
YM	Young's modulus
PR	Poisson's ratio
MPa	Mega Pascals

1. Introduction

Hydrocarbon exploration and production involve many challenges in the oil and gas industry; hence, it is important to study and understand petrophysical and geomechanical properties. Wellbore instabilities and subsidence of the wells and platforms are consequential problems due to a lack of geomechanical studies. Stress-induced wellbore instabilities are mainly observed from wellbore reduction, enlargement, and unintentional fractures due to excessive midweight. Majority of horizontal and deviated wells face stability issues while drilling through shale formations (Abass *et al.* 2006). Laboratory determination of geomechanical properties is essential to corroborate the log-based properties. Though the logs measure the data continuously with depth, it does not directly measure rock mechanical properties. Wellbore stability analysis for existing and future wells requires constructing and interpreting geomechanical models for the complete wellbore length (Zoback 2007). Generally, companies do not record the logs for the entire length of all wells drilled from the same platform. Developing mechanical earth models (MEM) for every individual well is indispensable for drilling mud design, improved and enhanced recovery methods.

Voids of missing wireline logs at different depths are filled by well correlation, core analysis, and-seismic-based results. Well correlations cannot accurately interpret the rock properties due to the formation's heterogeneity, but they always support core analysis and seismic methods. Studies on core samples have been carrying out from the 1930s (Ide 1937; Hughes and Cross 1951) to understand completely and determine the rock properties. Dynamic and static methods are two approaches used for determining the rock elastic properties in the lab. The stress–strain curve from compression tests is used for calculating static elastic constants, whereas the non-destructive sonic velocity measurements are often used for determining dynamic elastic constants of rock samples. Lab measurements of compressional wave (V_p) and shear wave (V_s) velocities are useful in finding the anisotropy of elastic properties, which helps in reservoir characterization (Riazi *et al.* 2017). In this paper, our objective is to set up a relation between the dynamic and static elastic properties and fill the void in the datasets to construct the one-dimensional MEMs for wellbore stability analysis. Core samples used for this study are gathered from the North-Heera field, Mumbai offshore. It is one of the largest producing offshore fields in the Asia Pacific region that started producing in the 1960s. Nearly 70 wells are drilled in this block from multiple offshore platforms; the core samples were provided from both exploratory and development wells. Heterogeneity and complexity of carbonate and shale formations make reservoir characterization difficult (Assefa *et al.* 2003). An integrated approach of determining wave velocities from seismic, ultrasonic measurements gives a stable relationship for calculating elastic properties (Garia *et al.* 2019). Velocities in the rock specimen depend on different parameters such as: (1) texture and lithology of the rock, generally in clay and shale formations have lower velocities; (2) saturation and type of fluid present in the pore spaces; (3) overburden pressure exerted on the sample, a steep increase of p-wave velocity with compaction; (4) change in temperature drops the velocity in both dry and saturated samples (Hicks and Berry 1956; Kassab and Weller 2011).

2. Methodology

Our objective is to analyze and interpret combined elastic properties determined from different methods considering petrophysical and sedimental features. Figure 1 illustrates our workflow, which includes measuring P-wave and S-wave velocities in the lab using 1 MHz longitudinal transducer and shear wave frequencies of 250 and 500 kHz; conducting triaxial compression tests to find the failure loads as wells as elastic properties; calculating elastic properties, principal stresses from the well-logs.

2.1 *Ultrasonic wave measurements*

Laboratory measurements of ultrasonic wave velocity (UVW) are the deep-rooted method to

measure the elastic properties of the rock samples. UVW was first practiced as far back as 1951 (Hughes and Cross 1951). In this research, ultrasonic testing has been carried out using two transducer pulse transmission technique (Birch 1960). In this study, to obtain the elastic properties, core plugs have been derived from different wells located in the North-Heera field, Mumbai. Elastic wave propagation depends on the rock elastic stiffness and density. In rock mechanics, elastic waves mean both the *primary* and *secondary* waves; only waves travel in both isotropic and homogeneous rock materials. P-wave velocity significantly varies in porous and non-porous materials also in dry and wet rocks. P-wave velocity is higher in saturated samples and lowers in dry samples, whereas S-wave velocity has lower water-saturated samples values (Kahraman 2007; Kassab and Weller 2015). Saturation has little effect on the S-wave velocity than P-wave velocity for highly compressive and very stiff materials. In the present investigation, collected core samples are mainly carbonates, shales, and a combination of both (Tao *et al.* 1995).

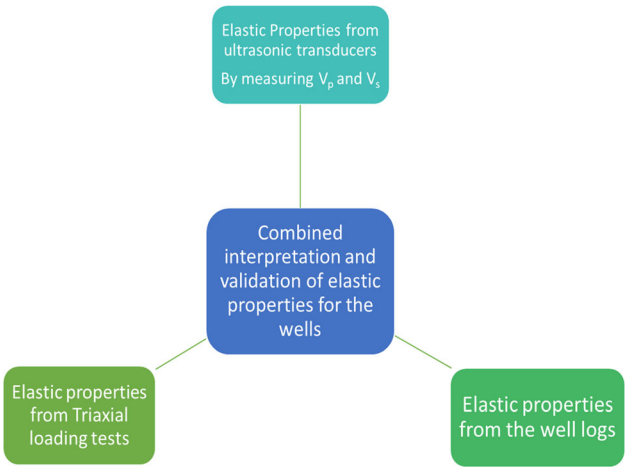

Figure 1. Details of the methodology to determine the elastic properties of reservoir rock from various methods.

Samples were prepared into smaller dimensions to improve the signal/noise ratio. For testing, core samples of 40 mm diameter and 70–80 mm length are prepared. Cylindrical core samples were made flat for transducer coupling, and prepared geologic samples were tested with ultrasonic RPR-4000 pulser/receiver in the ambient conditions. Ultrasound testing was carried out using transducers for compressional and shear wave frequency measurements (ASTM Int. 2000). Pulser transit time was measured using an oscilloscope display connected to the pulser/receiver, as shown in figure 2.

In the laboratory, transducers were placed in contact with the specimen's cylindrical surface to ensure the vibrations travelled through the core sample and picked up by the receiver. Firstly, the transducers were held tight on the specimen's cylindrical, smooth surfaces, and the travel time of the ultrasonic wave was measured. Transducers hold continuously onto the material's surface until a stable reading appears on the oscilloscope display, which is the time (t) in the microsecond (ms) for the ultrasonic pulse to travel the distance L. Moreover, the repeatability test has been performed by collecting each set of readings three times to ensure that the readings were repeatable and consistent.

As mentioned previously, typical ultrasonic transmission waveforms were recorded in UVW

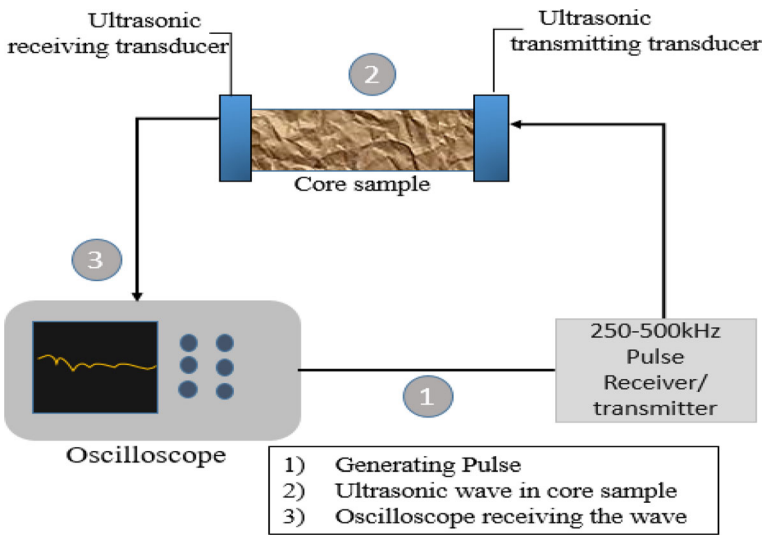

Figure 2. Schematic diagram of the experimental setup used for ultrasonic testing.

(a) **(b)**

Figure 3. (**a**) Cylindrical rock sample is inserted into the triaxial compression chamber and (**b**) conventional triaxial compression test setup equipped with strain gauges attached to the core sample specimen.

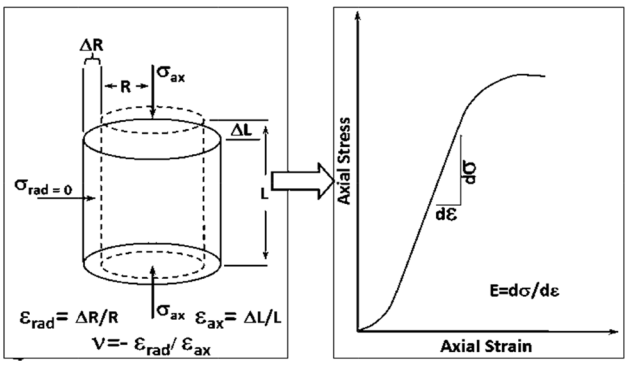

Figure 4. Modified cartoon illustration of rock deformation during the triaxial test and the axial stress and axial strain curve response (https://ofgeomech.com/).

experiments on core samples by P–P transducers and S–S transducers. If the measurements are done with P-transducers (figure 2), the pressure wave's travelling time was evaluated in terms of the moment of the first onset of energy. The pressure wave velocity is calculated as $V_p = L/T_p$, where T_p is the travelling time, which has been reflected in the oscilloscope display. The same approach has been employed to measure the shear wave's travelling time when S-transducers were used. A shear wave travelling time was evaluated, the arrival of the main beam with a high amplitude. Elastic constants of the rock samples are expressed in terms of wave velocities (Zoback 2007)

$$K = \rho v_p^2 - \frac{4}{3}\rho v_s^2, \tag{1}$$

$$V = \frac{v_p^2 - 2v_s^2}{2\left(v_p^2 - v_s^2\right)}, \tag{2}$$

$$E = \rho v_s^2 \frac{\left(3v_p^2 - 4v_s^2\right)}{\left(v_p^2 - v_s^2\right)}, \tag{3}$$

$$\mu = \rho v_s^2, \tag{4}$$

K, V, E, and μ are Bulk modulus (GPa), Poisson's ratio, Young's modulus (GPa) and shear modulus (GPa) respectively, ρ is bulk density (kg m^{-3}) of the rock specimen, v_p and v_s are compressional and shear wave velocities (m/s) measured in the rock sample in the lab.

2.2 *Triaxial compression tests*

The existing triaxial test method is one of the most effective ways to find the rock failure criteria and elastic properties in both petroleum and civil engineering disciplines. In this method, the elastic properties of the rock are determined by applying load from all three dimensions, and this method is static. Experiments were conducted on all the 10 core samples of 4″ diameter, used for ultrasonic measurements. In this study, conventional triaxial compression tests were carried out on an HRM592.201 digital compression testing machine having a load capacity of 1000 kN, where the confining pressures ($\sigma_1 > \sigma_2 = \sigma_3$) were used. Confining pressures in the triaxial cell are added in a sequence. Initially, confined pressure via hydraulic fluid is applied on the core sample (specimen) placed in a triaxial cell, later axial load is applied when the pressure inside the cell gets stabilized. Axial load continued to apply until the rock fails to take a further increase in load. In the

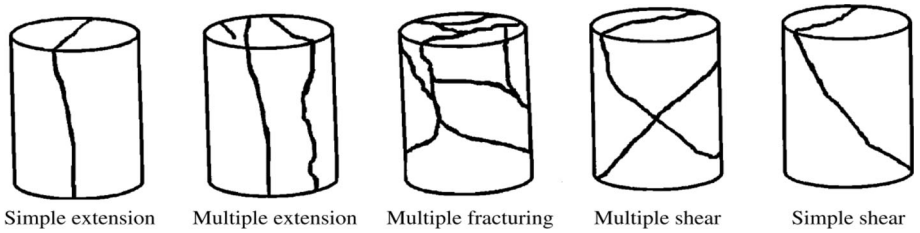

Figure 5. Modes of rock samples failure (Szwedzicki 2007).

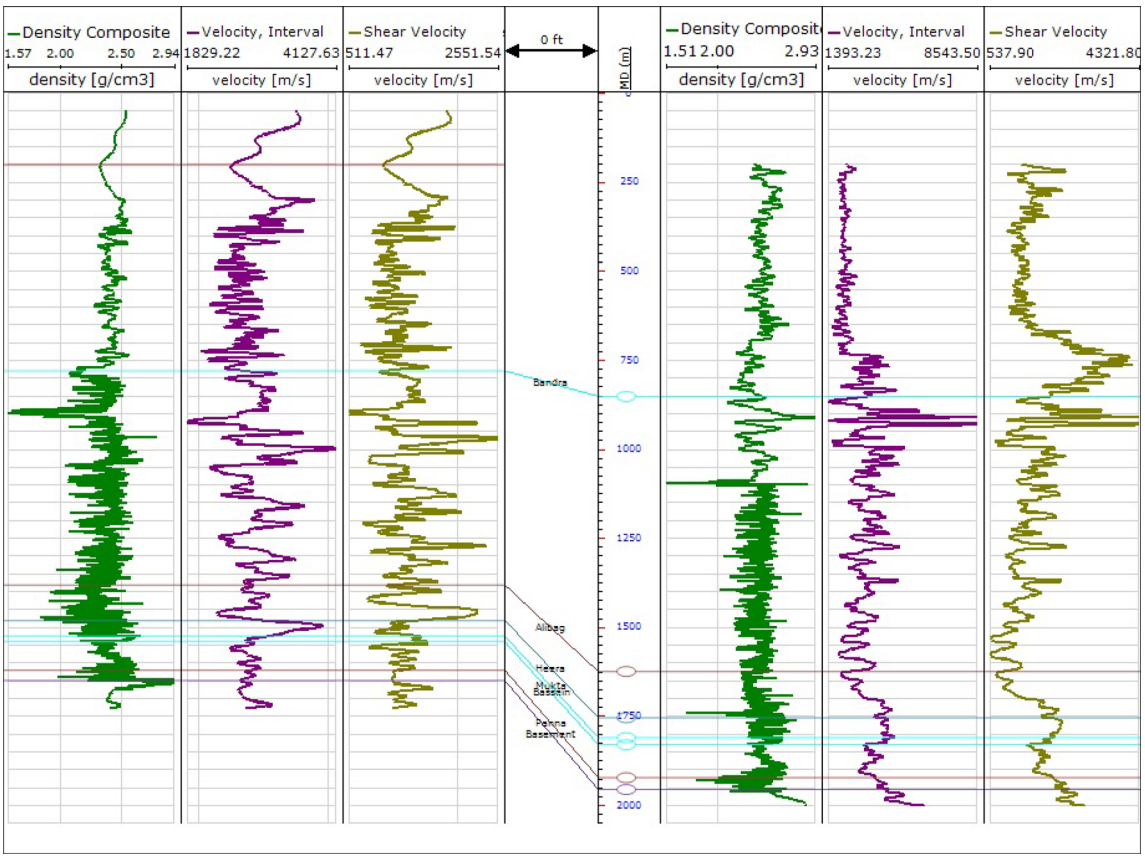

Figure 6. Well correlation view of density, P-wave and S-wave velocities of two different wells (vertical and directional) drilled from a same offshore platform.

past, the axial load was manually operated after rock failure. Triaxial compression units come with a computer-aided system, which controls the axial load after the collapse.

Rock failure parameters like cohesion (C_o) and the coefficient of internal friction angle (μ_i) are obtained from the Mohr–Coulomb failure envelopes at different confining pressures. Precise strain gauge probes are attached (shown in figure 3a) to monitor the amount of deformation (axial and lateral strain) in the rock samples using signal conditioning and data acquisition system. The strain is observed in both axial and radial directions (figure 4). A study of strain and deformation measurement has been performed in the same rock samples used for ultrasonic measurement. When the load is applied to the samples, they show different fracture deformation modes shown in figure 5. The differential signal from the axial and radial strain gauge is fed to two identical signal conditioning systems to be amplified and fed to the data acquisition system (DAQ2). The signal conditioning system is an embedded board that completes a single Wheatstone bridge in the quarter, half, or full bridge mode, and amplifies the signal giving a ground-referenced single-ended

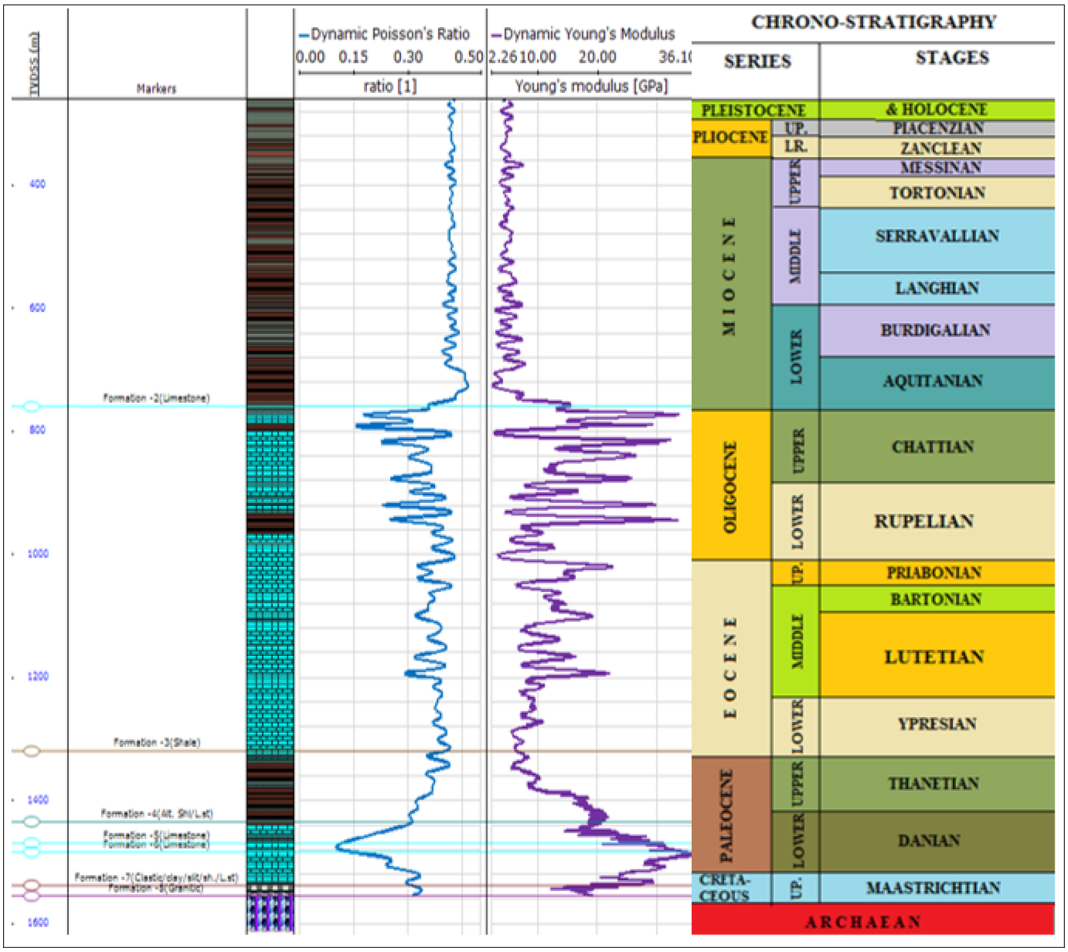

Figure 7. Dynamic Poisson's ratio and Young's modulus of a well-1 calculated from the wireline logs using lithology-based governing equations.

output. The gain and the offset of the signal conditioning board can be configured using the software. The two conditioning boards' voltage output is fed to two different channels of the data acquisition device (DAQ2), which is run in differential mode to cancel out common-mode noise. The strain gauge system is run in quarter bridge mode, with the strain gauge serving as one of the arms. Poisson's ratio (σ) and Young's modulus (E) are two elastic properties estimated from the stress–strain response curves (shown in figure 4) (Bieniawski and Bernede 1979; Fjaer *et al.* 1992).

Poisson's ratio is calculated from the ratio of slopes of both axial stress–axial strain curves, which is shown in the equation

$$v = \frac{-\Delta\varepsilon_r}{\Delta\varepsilon_z}. \tag{5}$$

Furthermore, Young's modulus of the rock is calculated directly from the slope of the axial stress–axial strain curves.

$$E = \frac{\Delta\sigma'_z}{\Delta\varepsilon_z}. \tag{6}$$

American Society for Testing and Materials (ASTM) and the International Society of Rock Mechanics (ISRM) have long-established standards for proper testing procedures to ensure reliable results for Young's modulus (E) and Poisson's ratio (σ).

2.3 *Elastic properties from well-logs*

Knowledge of mechanical properties of the rock formation and *in-situ* stresses calculations are crucial for analyzing wellbore stabilities, workover, and fracturing problems (Fjaer *et al.* 1992). Elastic properties are calculated from the well-logs. The dynamic elastic properties, Poisson's ratio (σ_{dy}) and Young's modulus (E_{dyn}) are determined basically from density and acoustic logs, which are shown in figure 6 (McNally 1987). The deformation

Age	Average Thickness (m)	Lithology	Seismic Marker	
Holocene to Pliocene	600	Clay and claystone	---	---
~~unconformity~~~~~~~~~~~~~~~~				
Late Miocene	250	Thick shale with minor limestone	---	---
~~unconformity~~~~~~~~~~~~~~~~				
Middle Miocene	70	Limestone with minor shale	L- I L-II	 Horizon-I
~~unconformity~~~~~~~~~~~~~~~~				
	300	Shale with prominent fine Sandstone, siltstone bands in The middle	S-I	------
Early Miocene ~~~~~~~~~~~~~~~~~~~~~~~~unconformity~~~~~~~~~~~~~~~~~~~~~~				
	470	Thick limestone with thin dark Grey and green shale	L -III	Horizon-II Horizon-III
Late Oligocene	100	Limestone/shale alternation	L - V	---------
~~unconformity~~~~~~~~~~~~~~~~				
Paleocene	10	Trap wash	-----	-------
~~unconformity~~~~~~~~~~~~~~~~				
		Basalt/Archean Metamorphics		

Figure 8. Lithology, age and thickness of the formations from the study block, where the shallow layers thick (600 m) shale and clay deposition from sea bed followed by thick limestone (800 m) with transition layers of shale at top and bottom, and the basement is basalt deposition in Paleocene age.

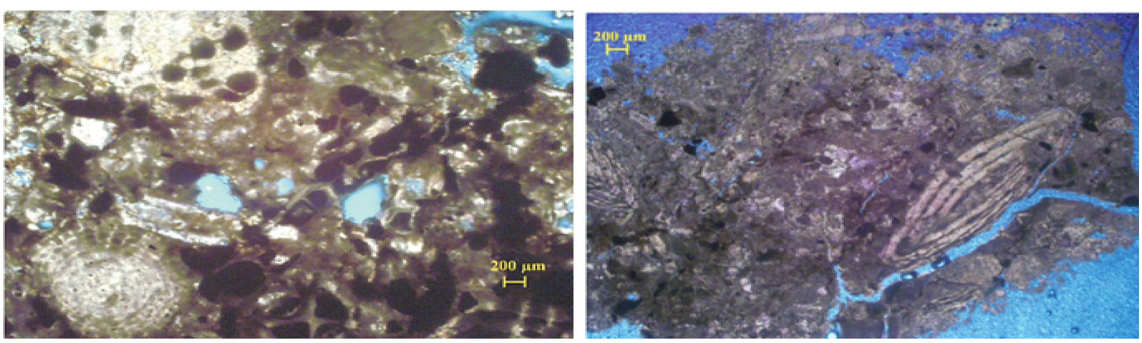

(a) **(b)**

Figure 9. Microscopic images of the limestone formation showing (**a**) vuggy porosity caused due to dissolution and (**b**) connectivity of the vuggy pores, which increases the permeability.

of rock is a slow process; hence for geomechanical analysis, static data are required. Near the wellbore in shallow sediments, rock behaves stiff under dynamic loading conditions. In this field, core samples are available for the calculation of static rock properties. After the core samples are tested for static properties, correlations are used to determine static Young's modulus and static Poisson's ratio for the total depth of a well (Fjar *et al.* 2008)

$$\sigma_{\mathrm{dy}} = \frac{V_p^2 - V_s^2}{2 \times \left(V_p^2 - V_s^2\right)}, \tag{7}$$

$$E_{\mathrm{dyn}} = \frac{\rho V_s^2 \left(3 V_p^2 - 4 V_s^2\right)}{\left(V_p^2 - V_s^2\right)}, \tag{8}$$

σ_{dy} and E_{dyn} are the dynamic Poisson's ratio, and Young's modulus in GPa, respectively. V_p and V_s are the compressional and shear wave velocities in km/s from the well logs, where ρ is the bulk density of the formation in kg m^{-3}. There are significant differences between static and dynamic Young's moduli. At low-stress levels, E_{dyn} is larger than static Young's modulus. Static Young's modulus (E_{sat}) can also be calculated

Table 1. *Petrophysical property of the shale rock core samples collected from the wells.*

Lithology	Porosity (%)	Permeability (mD)	Grain density (kg m^{-3})
Shale	5.57	0.01	2680
Shale	10.74	0.04	2720
Shale	6.57	0.01	2710
Shale	11.19	0.03	2740

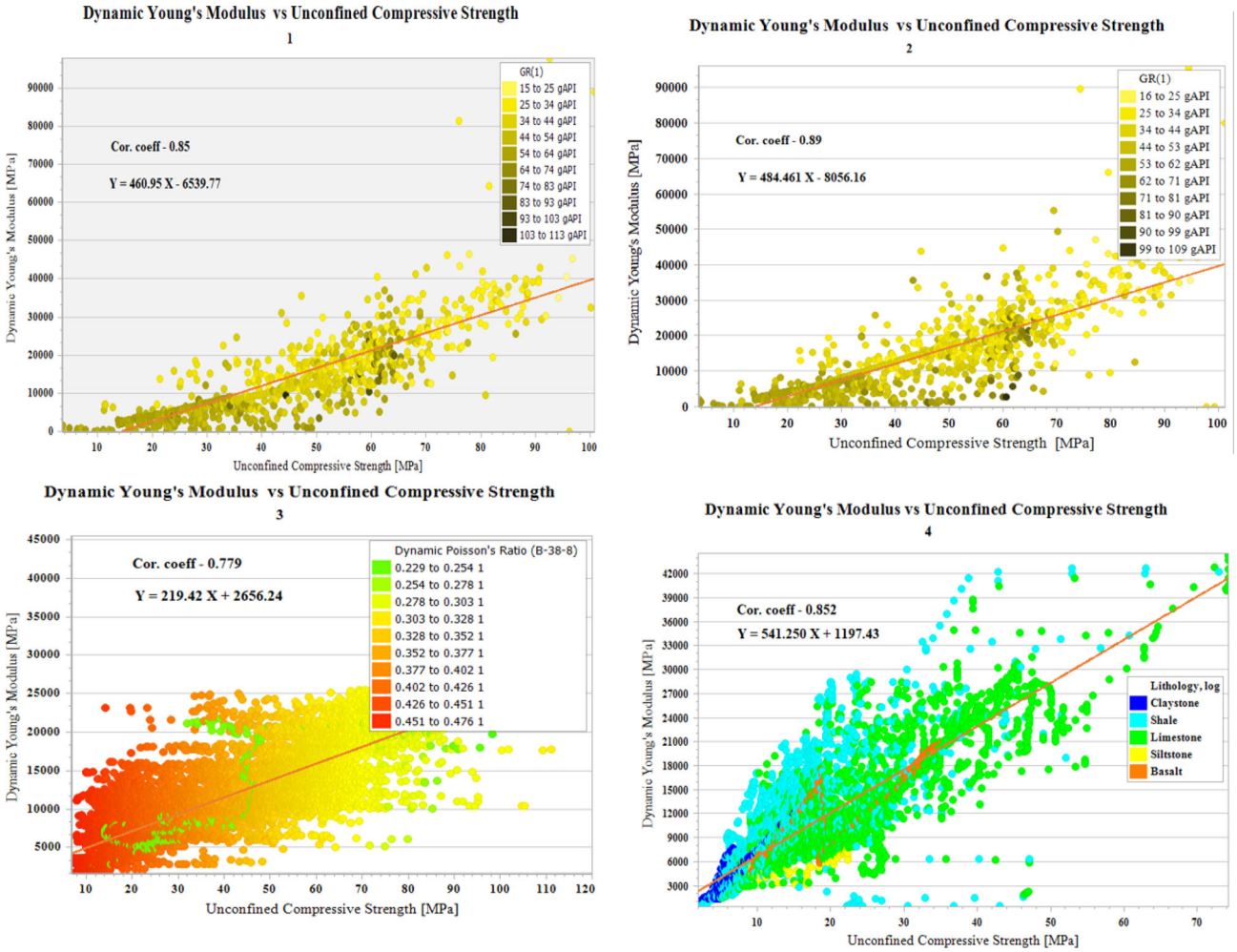

Figure 10. Correlation coefficients derived for different wells from cross plots of dynamic Young's modulus, unconfined compressive strength, fracture pressures, and Poisson's ratio.

using the wave velocities given in equation (6). As part of 1D MEM, rock static and dynamic properties are derived using the governing equations based on the formation's lithology (Zhang and Zhang 2017). The static elastic moduli and UCS are computed from the dynamic moduli calculated from the wireline logs using equations (9 and 10). The relation between static and dynamic moduli is lithology dependent, and the correlation coefficients used for the calculation of rock properties are obtained from the cross plot, as shown in figure 10. We used different empirical equations for different lithology types to calculate elastic moduli and UCS of the rocks. Different empirical equations estimated UCS for different lithology types using the elastic moduli of the rocks (Horsrud 2001; Chang *et al.* 2006; Fjaer *et al.* 2008).

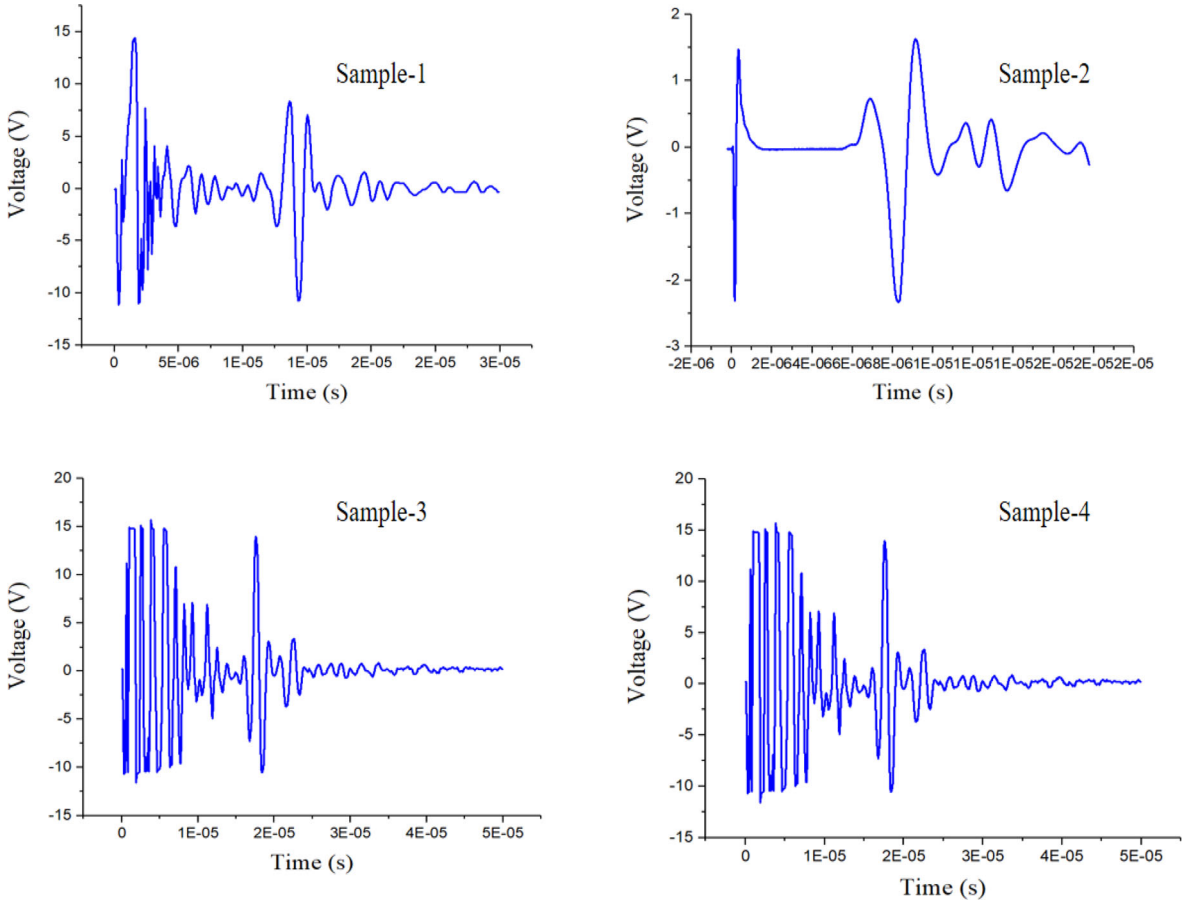

Figure 11. P-wave graph, energy and the sensor output (voltage) for measuring P-wave velocity.

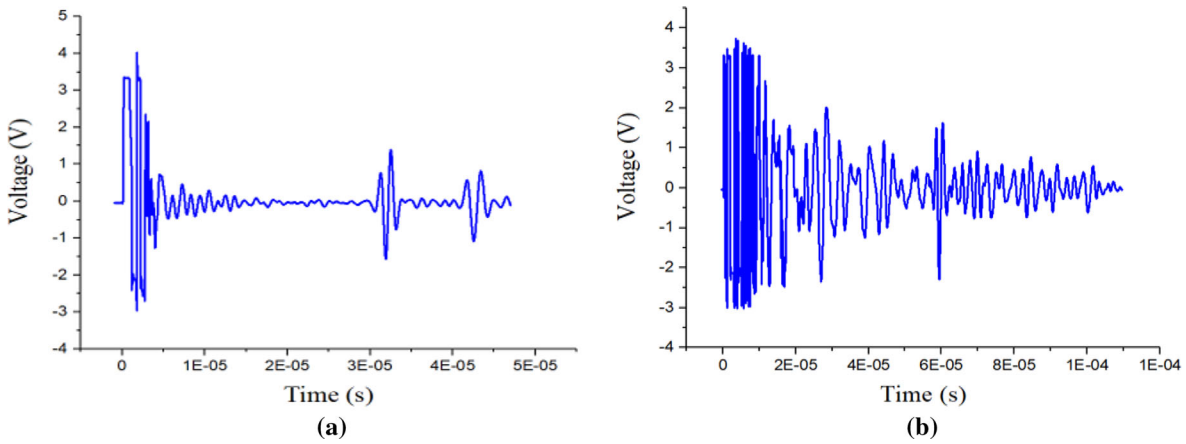

Figure 12. P-wave and S-wave measurements by the pulse-echo method, which addresses the high dynamic signals (noise) at the start of the measurement.

$$E_{\text{static}} = 0.06722 \times E_{\text{dyn}}^{1.0573}, \quad (9)$$

$$UCS_{\text{limestone}} = 4.66 \times E_{\text{dyn}}^{0.51}, \quad (10)$$

$$UCS_{\text{shale}} = 0.2215 \times E_{\text{dyn}}^{0.712}. \quad (11)$$

In the above equations, E_{dyn} and E_{static} are dynamic and static Young's modulus (figure 7).

3. Lithology and mineral information

Core samples are taken from the wells drilled from different platforms covering most of the North-Heera block. This block has an alternative series of shale and limestone formations, as shown in figure 1. Reservoir rock is composed of clastic and carbonate, and core samples are collected mainly

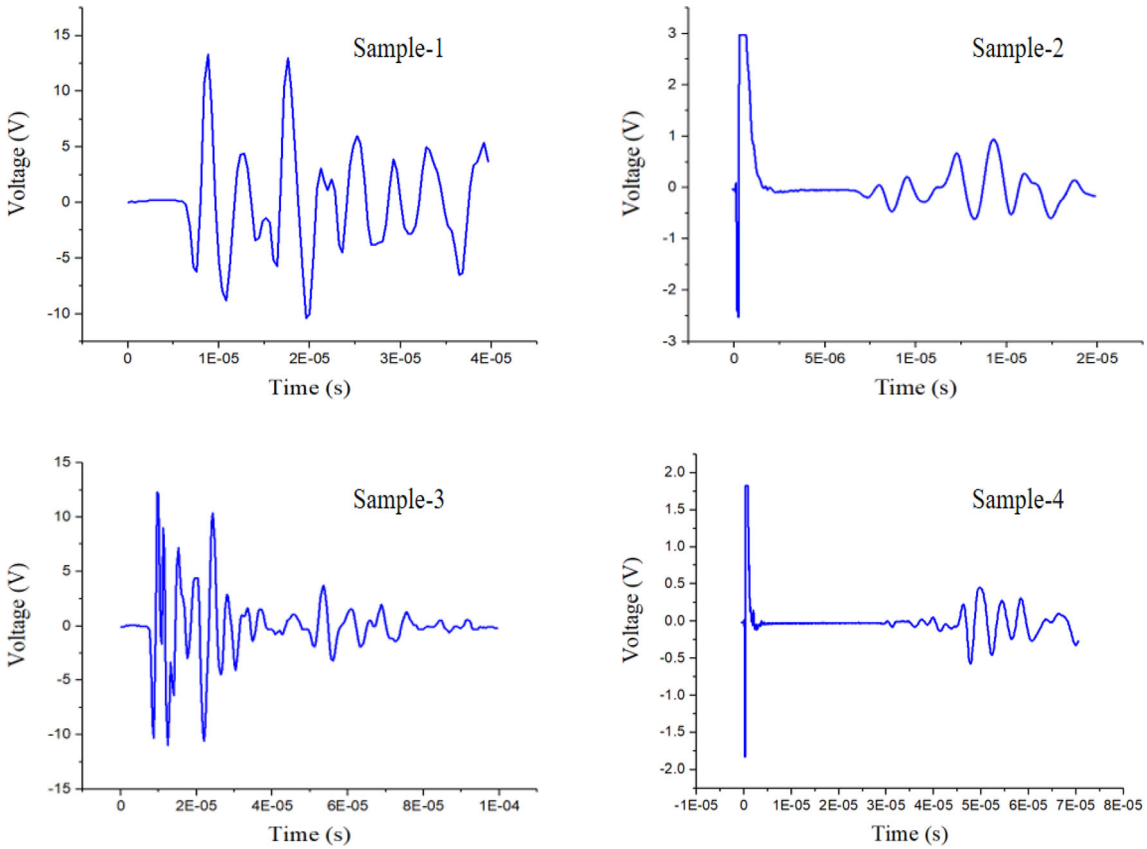

Figure 13. S-wave graph, energy and the sensor output for measuring S-wave velocity.

Table 2. *Density, V_p, V_s, and the elastic properties (Poisson's ratio, Young's modulus, bulk modulus, shear modulus) derived from the ultrasonic measurements in the rock samples.*

Sample type	Depth	Density (kg m^{-3})	V_p (m/s)	V_s (m/s)	Poisson's ratio	Young's modulus (GPa)	Bulk modulus (GPa)	Shear modulus (GPa)
Limestone	1538.5	2580	1615	907	0.27	5397	3950	2126
Limestone	1454	2110	1812	986	0.29	5299	4200	2054
Shale	1656	2550	1750	983	0.27	6250	4527	2466
Shale	1654	2260	1618	848	0.31	4263	3746	1627
Limestone	1557.4	2540	1647	854	0.31	4831	4172	1848
Limestone	1463.5	2510	1920	973	0.33	6315	6090	2379
Limestone	1541.5		1528	905	0.27	4705	3456	1848
Limestone	1545.2	2540	1748	979	0.27	6188	4513	2433
Limestone	1557	2330	1637	854	0.31	4452	3972	1695
Limestone	1560	2450	1688	872	0.31	4895	4335	1866
Basalt	1587.5	3110	1360	848	0.18	5286	2770	2236
Limestone	1554.7	2440	1671	884	0.31	4985	4276	1909
Limestone	1480		1142	553	0.35	2270	2474	846
Limestone	1481	2830	1606	744	0.36	4261	5204	1563

from depths 1100–1500 m ranging from lower Oligocene to middle Miocene as shown in figure 7. The shallow zone (formation-1) starts from the seabed, clay, and claystone with a zone thickness of 700 m. Formation-2 is carbonate mainly composed of limestone with vugular porosity and has a thickness of 600 m, followed by the formation-3, which is composed of shale with specky YF fluorescence formation-4 is alternative layers of shale and limestone. Formations 5 and 6 are pay zones

consisting of limestone, foraminiferal wackestone with patchy and vuggy porosity. Formation-7 below the pay zone is alternative layers of argillaceous limestone with interbedded shale, sandstone, and slit. Here, the shale is moderately hard, fissile, splintery, specks of pyrite crystal aggregates are seen along the bedding plane, feebly calcareous at places trending to claystone. Granitic layers (formation-8) below it is a basement rock shown in figure 8.

The core samples are mostly shale and carbonates, and porosity is one of the rock parameters that change the velocity. Carbonates have secondary porosities, which change the permeability; hence the microscopic studies are necessary for detailed pore and texture analysis. Microfacies of core samples showed that carbonates have secondary porosity, which is moderately vuggy at the top of the pay-zone and low vuggy porosity at the bottom of the pay-zone; tubular grains and vugs are micritized, and skeletal grains are sparitized as shown in figure 9(a). A very poorly fossiliferous and dissolution channel resulting in good channel porosity (permeability) is observed in the limestone illustrated in figure 9(b). The zones below the reservoir layers are mainly argillaceous limestone with interbedded shale. Here the shale is moderately hard, fissile, splintery, specks of pyrite crystal aggregates are seen along the bedding plane with porosity ranging from 5.57 to 11.19% and very low permeability, which are displayed in table 1.

4. Results and discussion

The conducted laboratory measurements set out the procedure for determining the ultrasonic wave velocity of different rock samples derived from different wells located in Mumbai's North-Heera field. Dry samples of shale, limestone, and basalt are tested in ambient conditions. Lithology information from well logs and core analysis provided the details of sediments and the mineralogy of the depositional environment. Velocity anisotropy is observed in the carbonate and shale samples from the ultrasonic measurements. The carbonate samples were taken from the same well; almost the same depth showed the different velocities shown in table 3. The strength anisotropies are noticed from the triaxial loading tests. Wellbore stability is analyzed from the rock elastic and strength parameters, pore pressure, and principal stresses. These parameters are calculated by governing equations from well logs considering the lithology changes with depth (figure 10). Based on the sample's length and travel time from the transmitter to the receiver, ultrasonic wave velocities were calculated. Moreover, we simultaneously calculated all static elastic constants from wireline logs. Figures 11–13 show the longitudinal velocity and shear wave diagrams for three samples where the wave spectrum changes with sensor output (oscillation) *vs.* time (seconds).

The velocity measurements are taken using the 250 and 500 kHz; the wave energy's quantitative changes are observed in sample-1, which is shale formation. Fourteen samples were tested for the velocity measurements, and the elastic properties (PR, YM, BM, SM) are calculated using equations (1–4). A significant difference in p-wave velocity is observed in the limestone samples ranging from 1142 to 1920 m/s, with an average of 1637 m/s. Average p-wave velocities measured in the shales and basalt samples are 1684 and 1360 m/s, respectively. S-wave velocities in the limestones have an average value of 865 m/s; shale samples have 915 m/s, as shown in table 2. Different empirical correlations estimated uniaxial compressive strength for different lithology types using the elastic moduli of the rocks. A typical triaxial test was carried out on digital compression testing machine with a load range capacity of 1000 kN to find the rock failure criteria on the test specimen with a height to diameter ratio of 2:1. In this study, the sample is subjected to stress conditions that attempt to simulate the *in-situ* stresses. Conventional triaxial compression tests are conducted on nine core samples (40 mm × 80 mm) derived from different depths from exploratory wells (vertical wells) and development wells. The samples have different sedimentary compositions; few samples are carbonate-rich type, and few samples are a combination of shale and carbonates. Samples from depths 1000–1200 m are mainly composed of shale, below 1200 m, it is primarily carbonate and a combination of shales and carbonates. Maximum (σ_1) and minimum (σ_3) stresses are applied to the sample in the triaxial cell until the failure of the sample. Triaxial compression tests on the core samples resulted in different modes of fractures such as simple shear, multi shear, multiple extension, shear extension fractures. Figure 14(a–e) shows the different lithology samples that exhibited different fracture modes under different confining pressures. Figure 14(a, d) is mainly shale and limestone dominant samples, respectively, which

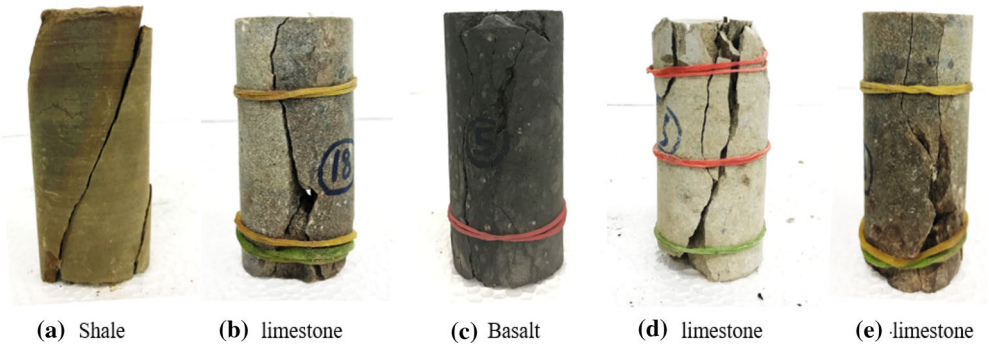

Figure 14. Different failure modes of the rock samples during the compression triaxial loading tests.

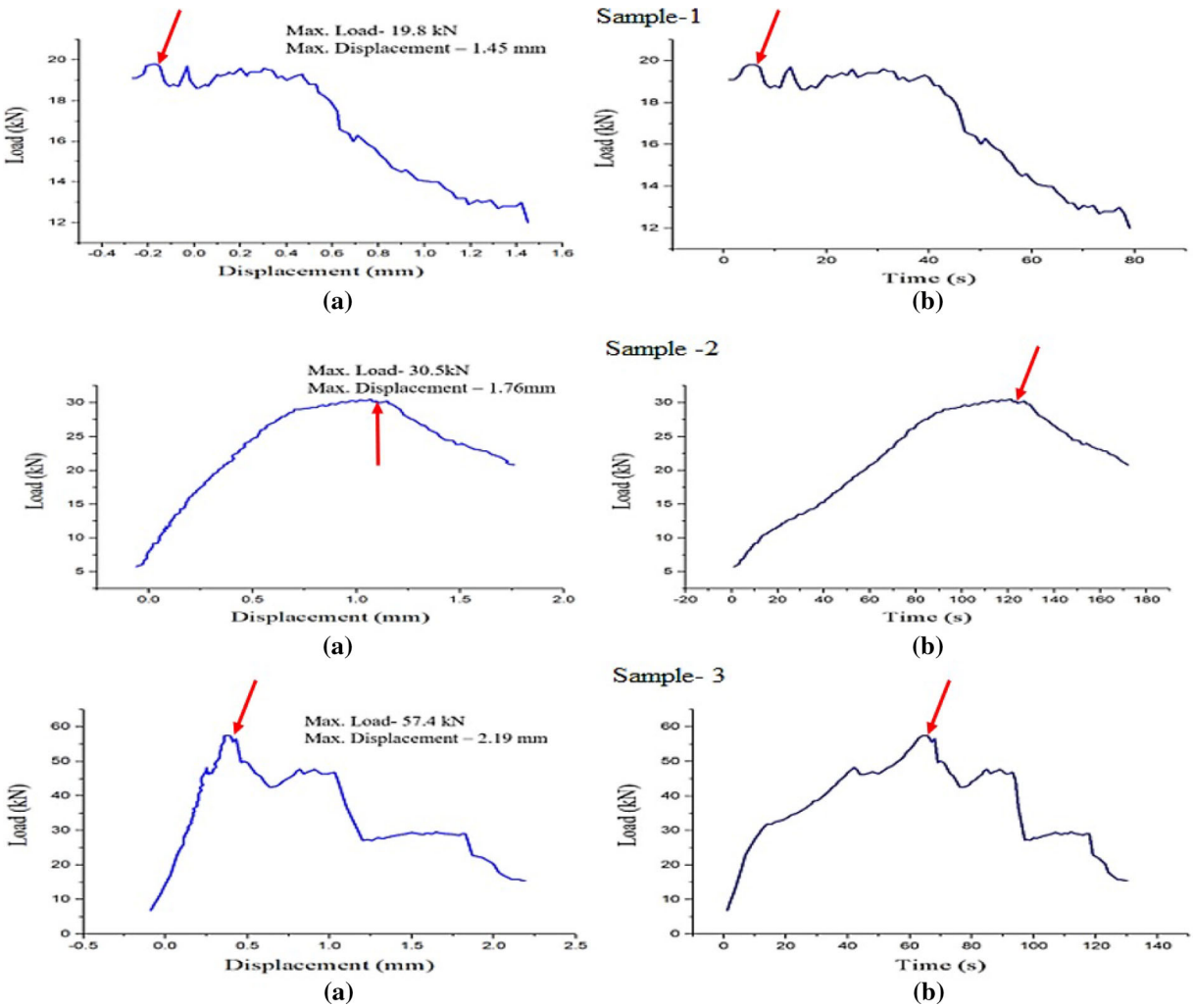

Figure 15. Stress and strain response curves for different samples (**a**) illustrates displacement of the specimen with the load and (**b**) illustrates the graph of load (kN) *vs.* time (sec); the maximum during the test is marked by the red arrow.

displayed the shear failure, figure 14(b, e) is limestone samples and they have undergone a multi-axial splitting phenomenon, whereas figure 14(c) is basalt and which is a basement rock for the reservoir exhibited a multi-shear failure. As discussed in the earlier section through equations (5–6) about obtaining Poisson's ratio and Young's modulus from the stress–strain graph's slope. Displacement of the rock with load and the increment of pressure applied on the core sample inside the triaxial cell with time is shown in figure 15. The loading path is given for corresponding samples during the triaxial loading test, the cylindrical rock sample first revealed linear elastic behaviour and then

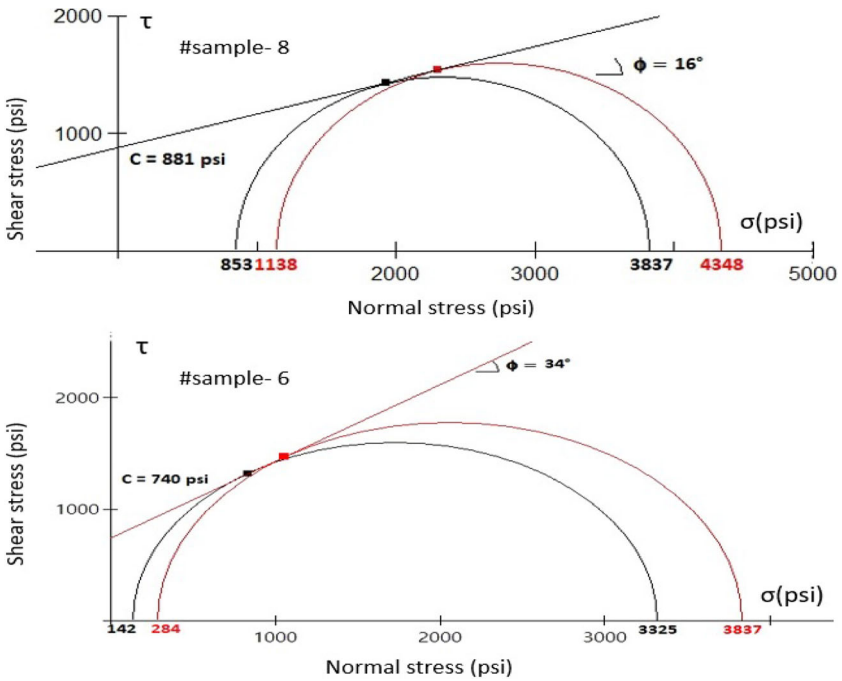

Figure 16. The Mohr–Coulomb failure plot for the samples taken from different depths, and cohesion and friction angle are calculated from the Mohr circles and tangent.

Table 3. *Confining pressures applied during the triaxial loading tests and the rock parameters (internal friction angle, μ_i, and cohesion, C_o) obtained using Mohr–Coulomb failure envelopes from test results.*

Sample no.	Depth (m)	σ_1 (psi)	$\sigma_2 = \sigma_3$ (psi)	Internal friction angle μ_i (degree)	C_o cohesion (psi)
1	1000–1100	2491.90	450	27.32	389.30
2	1000–1100	2792.08	550	31.03	303.44
3	1250–1260	6298.34	650	40.266	758.383
4	1345–1350	5344.8	625.11	32.947	877.574
5	1445–1450	4348.15	560.80	32.99	877.5
6	1535–1540	53,330.36	700	34.431	740.892
7	1535–1540	10,230.80	711.167	52.89	605.17
8	1552–1560	3238.051	426.70	18.01	881.58
9	1580–1585	8952.7	853.50	27.32	622.93

elastoplastic behaviour. The two curves of samples in figure 15 are identical in describing the growth of the crack. The curve indicates the linear behaviour till the maximum load of 30.5 KN is achieved, then the behaviour is entirely nonlinear from crack initiation until fracture point. All the curves reflect the nonlinear behaviour after the maximum load is achieved. At failure condition, cohesion and friction angle along the rupture surface, are obtained from the Mohr–Coulomb criterion (shown in figure 16) at different confining pressures shown in table 3. Young's modulus of the rock was calculated directly from the axial stress–strain curve's average slope. Generally, the P-wave velocity decreases with the increase in porosity, where the limestone samples used for this study are taken from the reservoir layers. The lithology of this block has the shale layers at shallow depths and is followed by alternative layers of limestone and shale to the depth of 1450 m. Limestone reservoirs are thin layers and compact followed by layer of shale, slit and sandstone, the increase in the P-wave velocity may be occurred due to the depositional process. The cross plots of density *vs.* P-wave velocity logs are created for two vertical wells, an increase in the velocities are observed at the depths 1450–1550 m as shown in figures 17 and 18(a).

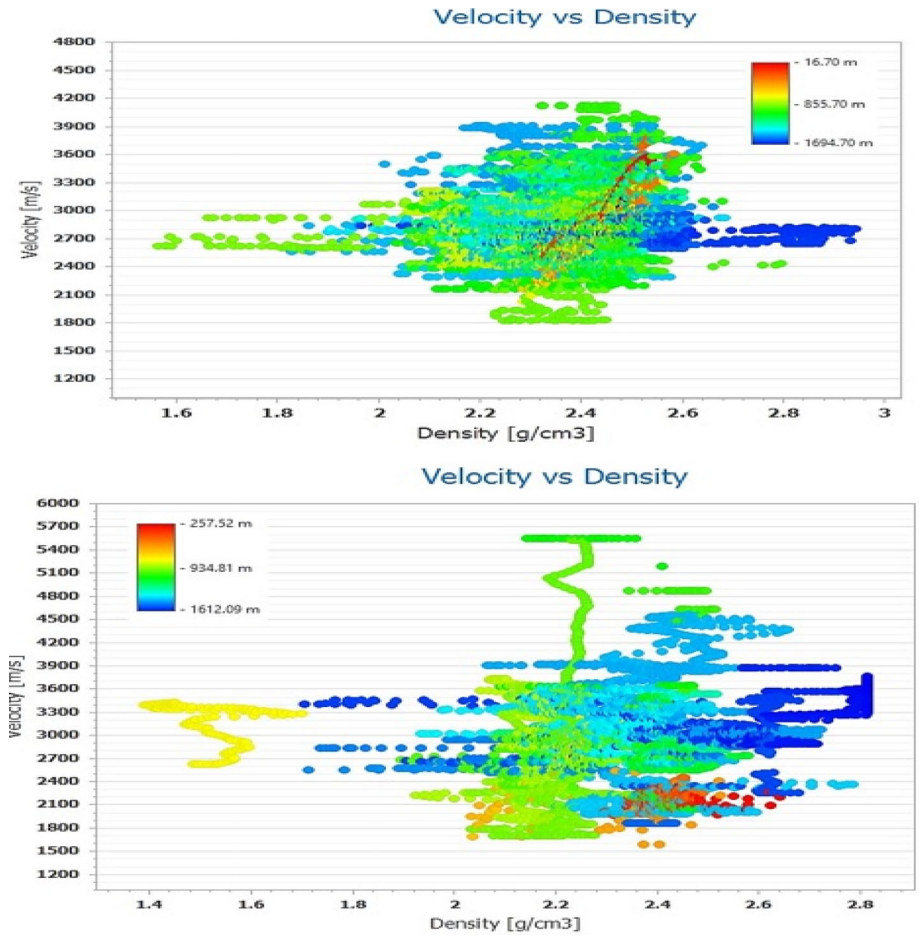

Figure 17. Cross plots of density and P-wave velocity for two vertical wells drilled in the study block; an increase in the velocities are noticed at a depth interval of 1400–1500 m.

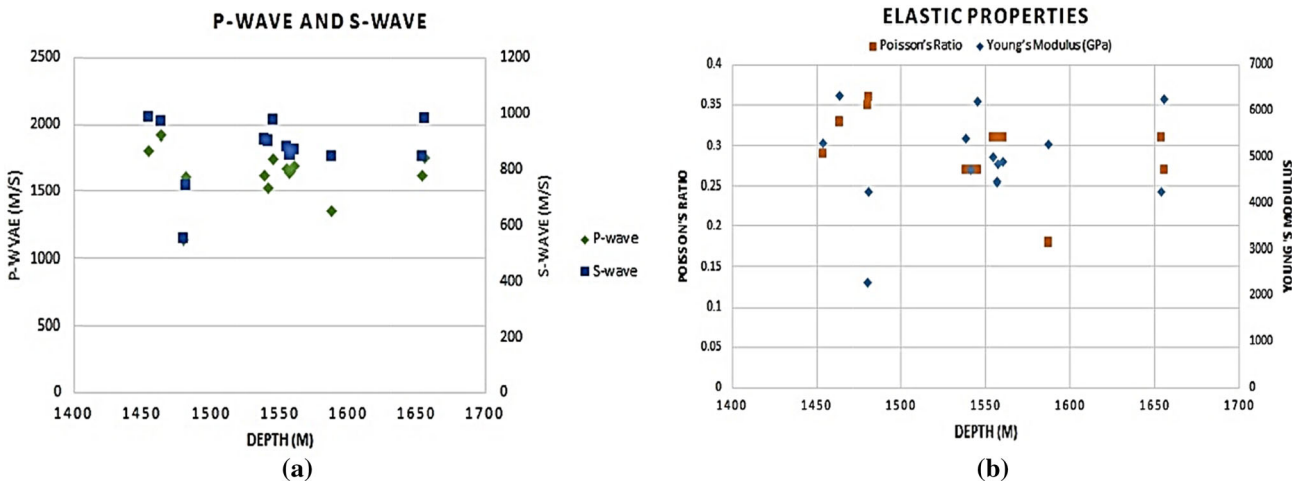

Figure 18. (**a**) P-wave and S-wave velocities measured from the ultrasonic methods, a decrease in velocities are observed in the depth interval (1450–1500 m), (**b**) YM and PR plot with depth estimated from the laboratory methods.

Well logs are the primary inputs for calculating dynamic elastic properties for the wellbores. The gamma-ray log was used for the lithology identification, constants in equations (7–8) are formulated to determine the elastic properties that are primarily lithology dependent. The cross plot is created for the PR and YM estimated from ultrasonic methods (figure 18b), and the values varied in the

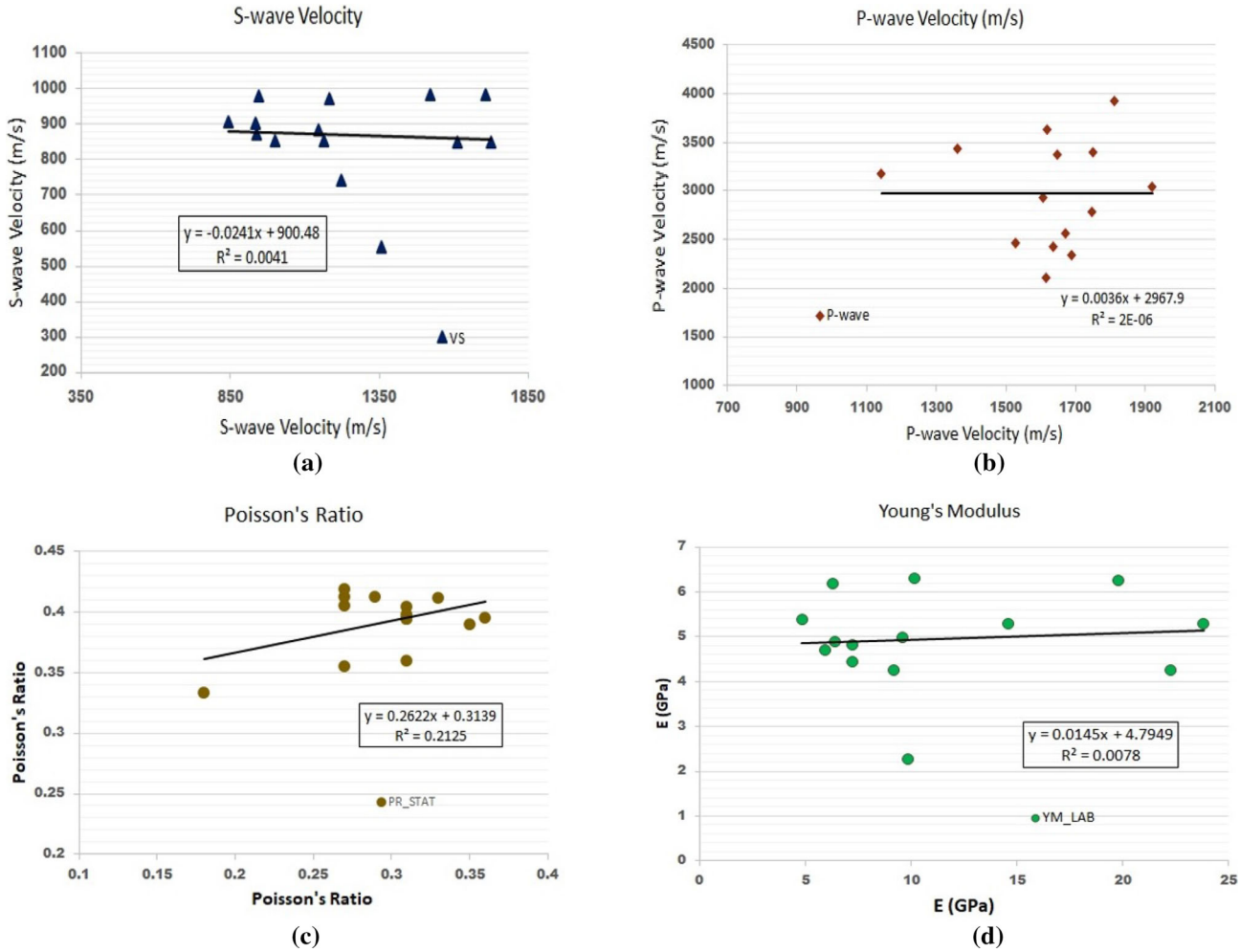

Figure 19. (**a**) Cross-plot of static and dynamic S-wave velocity; cross-plot of static and dynamic elastic properties, (**b**) Cross-plots of static and dynamic P-wave velocity at the study area between the depths of 1400 and 1600 m, (**c**) cross-plot of static and dynamic Poisson's ratio from the depth interval of 1400–1600 m, and (**d**) cross-plot of static and dynamic Young's modulus.

limestone layers (1400–1500 m). Well markers, seismic horizons were used for setting up the lithology layers and transition zones (figure 19). Figure 20 shows the dynamic elastic properties along the well path for well-1. There are many fluctuations in the trends of Young's modulus, Poisson's ratio, and UCS. The average value of YM in the shale (formation-1) up to 790 m is 2.5–8 MPa, and PR is 0.38–0.45 as shown in figure 20. Significant changes in the elastic properties are observed in the shale-carbonate transition zones. The relation between UCS, Poisson ratio, and Young's modulus with reference to lithology is derived for the wells from different platforms. Correlation coefficient of UCS and YM for the wells ($R^2 = 0.85$, 0.89, 0.779, 0.852) is shown in figure 10. Cross plots for the static and dynamic elastic properties and velocities are plotted, and the relation between them is estimated which is shown in figure 19.

5. Conclusions

Geomechanical testing has been carried out using triaxial tests with ultrasonic measurements on different rock samples derived from different wells located in the North-Heera field, Mumbai. The objective is to analyse the wellbore stability by estimating rock elastic properties such as Poison's ratio (PR_{dy}), Young's modulus (E_{dyn}), Bulk modulus (K), shear modulus (G), and unconfined compressive strength (UCS) from well logs, ultrasonic measurements and triaxial loading tests. In the process, the voids in the well logs are filled and calibrated from the laboratory results. The

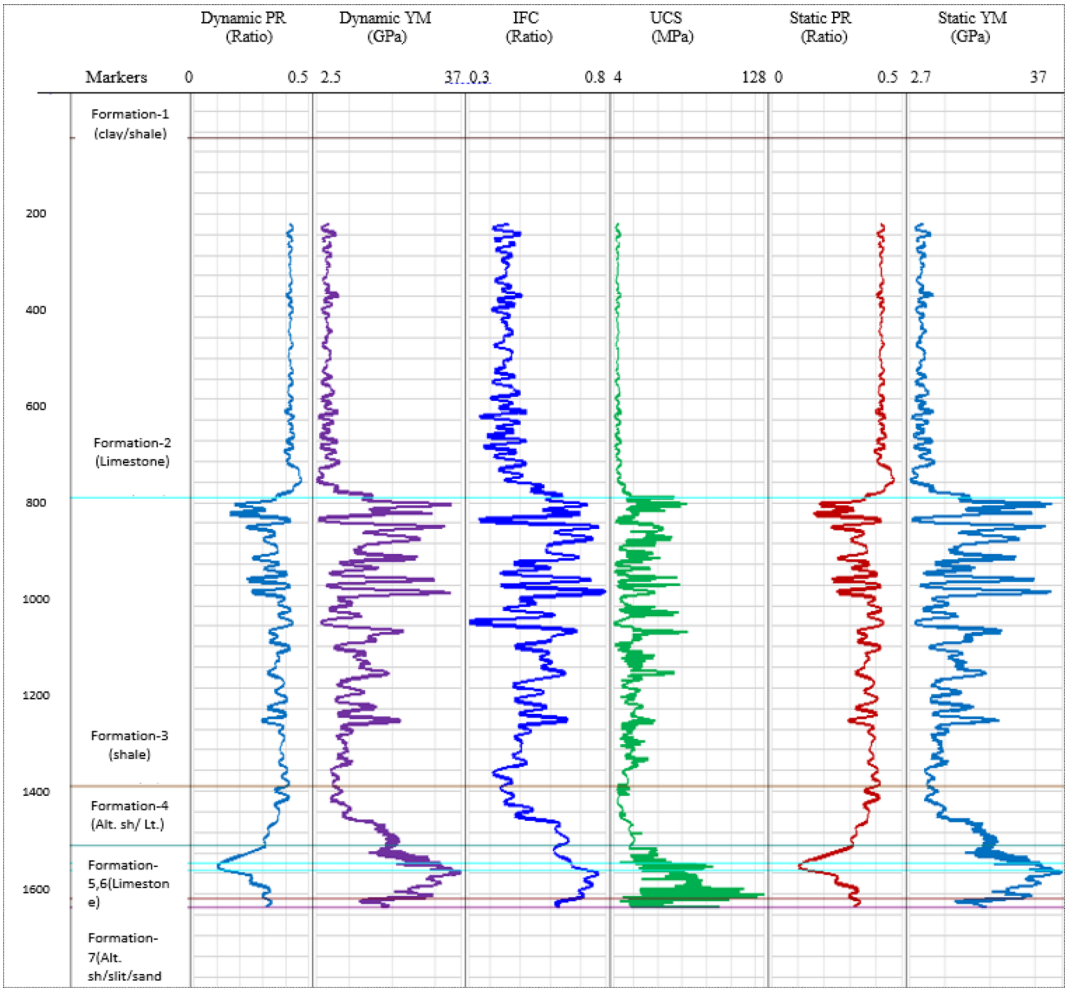

Figure 20. Rock properties (dynamic Poisson's ratio, dynamic Young's modulus, internal friction coefficient, UCS, static Poisson's ratio, static Young's modulus) of well-1.

ultrasonic wave velocity is a qualitative evaluation approach for wave energy, and core sample failure is an energy dissipation and transfer process in a triaxial testing method. The triaxial experiments involve applying high confining pressure and a broad range of stress states on the rock samples. Integrated analysis of dynamic rock properties from well logs and interpretation of elastic properties from triaxial and ultrasonic methods imparted a forward way to a comprehensive understanding of rock anisotropy and wellbore instabilities. Cross plots of elastic properties and strength parameters, it is very much understandable that shales from shallow depth with high gamma-ray values show low UCS and low dynamic YM.

Moreover, 1D mechanical Earth models represent the rock properties, pore pressure, *in-situ* stresses, stress direction, and failure criteria of wellbore calculated from wireline logs. Mineral composition, shale anisotropy, seismic velocities, and cross plots are studied to understand shear wave splitting. In line with the research findings derived from the present study, the major conclusions are given below:

- In ultrasonic testing, a significant difference in P-wave velocity is observed in the limestone samples ranging from 1142 to 1920 m/s, with an average of 1637 m/s. Average P-wave velocities measured in the shales and basalt samples are 1684 and 1360 m/s, respectively. S-wave velocities in the limestones have an average value of 865 m/s; shale samples have 915 m/s.
- A relation among the elastic properties and strength parameters is established from cross plots for a better understanding of rock strength anisotropies.
- In a triaxial compression test, energy consumption during rock structural failure results in the crack initiation, propagation, and failure of rock

samples. In these tests, the modes of fracture were simple, and multiple shears and various shear extensions.

- In the 1D MEM study, the average value of Young's modulus in shale formation is around 2.5–8 MPa, and the Poisson ratio of 0.38–0.45 up to 790 m depth. Significant changes in the elastic properties have been discovered in the multilayered shale-carbonate transition zones.

Despite difficulties in preserving and replicating the field conditions of the core samples, elastic properties derived from the ultrasonic measurements (dynamic) and triaxial compression tests (static) have a close range with the elastic properties calculated from the well logs. This study provides insights of comparison of elastic properties which provide the information for future analysis of the wells where the data are unavailable for this reservoir block.

Acknowledgements

Authors extend their gratitude to Oil and Natural Gas Corporation Limited (ONGC) and Baker Hughes for their continuous support to make this research work possible and thank ONGC-Mumbai and CEWELL-Baroda for providing data for this research under the PAN IIT project. We also thank our supervisor for his uninterrupted support and for providing the lab facilities for conducting the experiments.

Author statement

Venkatesh Ambati: Performed the lab and analytic calculations and computations, implemented and interpreted the study, and contributed in the write-up of initial and final version of the paper. Shashank Sharma: Carried out the lab experiments, contributed in analytical work, visualization, data curation, and write-up of the initial version. Nagendra Babu M: Contributed in data analysis, interpreting the results and worked on the final draft preparation. Rajesh R Nair: Designed the study, project administration, interpretation of complete results, write-up of final version of the manuscript and overall supervision of the work.

References

Abass H, Shebatalhamd A, Khan M, Al-Shobaili Y, Ansari A, Ali S and Mehta S 2006 Wellbore instability of shale formation: Zuluf Field, Saudi Arabia; Paper presented at the SPE Technical Symposium of Saudi Arabia Section, Dhahran, Saudi Arabia, https://doi.org/10.2118/106345-MS.

Assefa S, McCann C and Sothcott J 2003 Velocities of compressional and shear waves in limestones; *Geophys. Prospect.* **51** 1–13, https://doi.org/10.1046/j.1365-2478.2003.00349.x.

ASTM Int 2000 Laboratory determination of pulse velocities and ultrasonic elastic constants of rock; *Designation: D* 2845-00 **14** 1–9.

Bieniawski Z T and Bernede M J 1979 Suggested methods for determining the uniaxial compressive strength and deformability of rock materials: Part 1. Suggested method for determining deformability of rock materials in uniaxial compression; *Int. J. Rock Mech. Min. Sci. Geomech. Abstr.* **16** 138–140, https://doi.org/10.1016/0148-9062(79)91451-7.

Birch F 1960 The velocity of compressional waves in rocks to 10 kilobars: 1; *J. Geophys. Res.* **65(4)** 1083–1102, https://doi.org/10.1029/JZ065i004p01083.

Chang C, Zoback M D and Khaksar A 2006 Empirical relations between rock strength and physical properties in sedimentary rocks; *J. Pet. Sci. Eng.* **51** 223–237, https://doi.org/10.1016/j.petrol.2006.01.003.

Fjaer E, Holt R M, Horsrud P, Raaen A M and Risnes R 1992 *Petroleum Related Rock Mechanics*, 1st edn, Elsevier Science Publishers, **33** 337p.

Fjaer E, Horsrud P, Raaen A M and Holt R M 2008 *Petroleum Related Rock Mechanics*, 2nd edn, Elsevier Science Publishers, **53** 514p.

Garia S, Pal A K, Ravi K and Nair A M 2019 A comprehensive analysis on the relationships between elastic wave velocities and petrophysical properties of sedimentary rocks based on laboratory measurements; *J. Pet. Explor. Prod. Technol.* **9** 1869–1881, https://doi.org/10.1007/s13202-019-0675-0.

Hicks W G and Berry J E 1956 Application of continuous velocity logs to determination of fluid saturation of reservoir rocks; *Geophysics* **21** 739–754, https://doi.org/10.1190/1.1438267.

Horsrud P 2001 Estimating mechanical properties of shale from empirical correlations; *SPE Drill. Complet.* **16** 68–73, https://doi.org/10.2118/56017-PA.

Hughes D S and Cross J H 1951 Elastic wave velocities in rocks at high pressures and temperatures; *Geophysics* **16** 577–593, https://doi.org/10.1190/1.1437706.

Ide J M 1937 The velocity of sound in rocks and glasses as a function of temperature; *J. Geol.* **45** 689–716, https://doi.org/10.1086/624595.

Kahraman S 2007 The correlations between the saturated and dry P-wave velocity of rocks; *Ultrasonics* **46** 341–348, https://doi.org/10.1016/j.ultras.2007.05.003.

Kassab M A and Weller A 2011 Porosity estimation from compressional wave velocity: A study based on Egyptian sandstone formations; *J. Pet. Sci. Eng.* **78** 310–315, https://doi.org/10.1016/j.petrol.2011.06.011.

Kassab M A and Weller A 2015 Study on P-wave and S-wave velocity in dry and wet sandstones of Tushka region, Egypt; *Egypt. J. Pet.* **24** 1–11, https://doi.org/10.1016/j.ejpe.2015.02.001.

McNally G 1987 Estimation of coal measures rock strength using sonic and neutron logs; *Geoexploration* **24** 381–395, https://doi.org/10.1016/0016-7142(87)90008-1.

Riazi N, Clarkson C R, Ghanizadeh A, Vahedian A, Aquino S and Wood J M 2017 Determination of elastic properties of tight rocks from ultrasonic measurements: Examples from the Montney Formation (Alberta, Canada); *Fuel* **196** 442–457, https://doi.org/10.1016/j.fuel.2017.01.084.

Szwedzicki T 2007 A hypothesis on modes of failure of rock samples tested in uniaxial compression; *Rock Mech. Rock Eng.* **40** 97–104, https://doi.org/10.1007/s00603-006-0096-5.

Tao G, King M S and Nabi-Bidhendi M 1995 Ultrasonic wave propagation in dry and brine-saturated sandstones as a function of effective stress: Laboratory measurements and modelling; *Geophys. Prospect.* **43** 299–327, https://doi.org/10.1111/j.1365-2478.1995.tb00255.x.

Zhang Y and Zhang J 2017 Lithology-dependent minimum horizontal stress and in-situ stress estimate; *Tectonophys.* **703** 1–8, https://doi.org/10.1016/j.tecto.2017.03.002.

Zoback M D 2007 *Reservoir Geomechanics*; Cambridge University Press, Cambridge, https://doi.org/10.1017/CBO9780511586477.

Corresponding editor: N V Chalapathi Rao